JOURNAL OF MATERIALS SCIENCE **34** (1999) 509–513

Dynamic tensile properties of Ti–47Al–2Mn–2Nb alloy

Y. WANG, D. LIN (T. L. LIN)*
Department of Materials Science, Shanghai Jiaotong University, Open Laboratory of Education Ministry for High-Temperature Materials and Tests, Shanghai, 200030, P.R. China
E-mail: dllin@mail.sjtu.edu

Y. ZHOU, Y. XIA
Department of Modern Dynamics, University of Science and Technology of China, Hefei, Anhui Province, 230026, P.R. China

C. C. LAW
Materials and Mechanics Engineering, United Technologies Corporation–Pratt & Whittney, 400 Main Street, East Hartford, CT 06108, USA

Room temperature tensile properties of polycrystal Ti–47Al–2Mn–2Nb alloy with near lamellar (NL) microstructures were investigated at the strain rates between 10^{-5} and $1000\,s^{-1}$ using a self-designed Split-Hopkinson tensile bar setup with a rotating disk and conventional testing machine. It was found that tensile ductility varies within a narrow range with the strain rate, while dynamic strengths (σ_d) of the alloy are obviously higher than static strengths (σ_s). There exists linear relationship between σ_s and the logarithm of the strain rate ($\ln\dot{\varepsilon}$), and between σ_d and the strain rate itself ($\dot{\varepsilon}$). Fractography analysis indicates that the alloy fractures in a mixed mode of predominant transgranular cleavage and minor intergranular cracking under static and dynamic strain rates. Environmental effect is excluded from the main cause for the room temperature brittleness of the investigated alloy.

1. Introduction

Two-phase γ titanium aluminides, which are composed of a major phase of γ–TiAl and a minor phase of α_2–Ti_3Al, are receiving increasing attention because of their high specific strength and stiffness, excellent oxidation resistance, and low density [1]. As the alloys are expected to be used as structural materials, their mechanical properties have been investigated intensively and extensively. However, the investigation is far from being complete. In the course of machining and future utilization, TiAl alloys are possibly subjected to dynamic or shock loads, which necessitates the knowledge of mechanical properties at high strain rates, or dynamic strain rates. Unfortunately, most of the numerous research efforts conducted up to now on the mechanical properties of TiAl alloys are limited to static or quasi-static loading, whose strain rates are less than $10^{-1}s^{-1}$. Chin *et al*. [2] and Maloy *et al*. [3–7] investigated mechanical response to dynamic compression in Ti–48Al–(5∼15) vol % TiB_2 and in some intermetallic alloys, including Ti–48Al–2Nb–2Cr under the strain rates of 500 and 2000 s^{-1}, respectively. More recently, Wang *et al*. [8] and Chen *et al*. [9, 10] investigated dynamic tensile properties of Fe_3Al [8], Ni_3Al [9] and polysynthetically twined (PST) TiAl alloys [10] using a self-designed Split-Hopkinson tensile bar (SHTB) setup and found some interesting dynamic tensile behaviors of the investigated intermetallics. In this paper, the same SHTB setup is used to study tensile properties of polycrystaline Ti–47Al–2Mn–2Nb alloy with near lamellar microstructure under the strain rates between 20 and $10^3\,s^{-1}$. For comparison, static tensile properties of the same alloy are also investigated using conventional tensile techniques.

2. Experimental procedures

The investigated alloy, referred to TiAlMnNb alloy hereafter, has chemical composition of Ti–47 at % Al–2 at % Mn–2 at % Nb. Its preparation has been accounted for elsewhere [11]. Its initial microstructure was etched by a mixture of 2.5 vol %HF + 2.5 vol % HNO_3 + 95 vol %H_2O and observed by a Neophot–II optical microscope.

Plate tensile specimens were cut from the plates by EDM (electro-discharging machining) and then the surfaces were carefully ground to about 0.5 mm deep using emery paper to remove the damaged materials. Finally, the specimens were electro-polished to remove surface scratches [11]. Static tensile tests were conducted on a

* To whom all correspondence should be addressed.

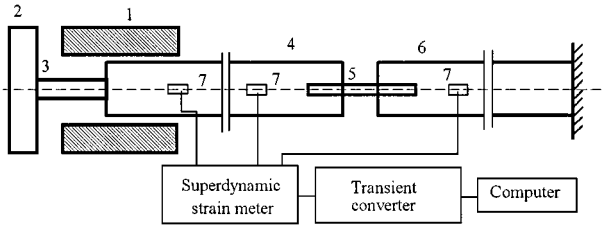

Figure 1 Sketch of dynamic tensile setup 1—hammer 2—block 3—short metal bar 4—input bar 5—specimen 6—output bar 7—strain gauges.

Shimadzu AG–100kNA testing machine at room temperature under the strain rates of 10^{-5}, 10^{-4}, 10^{-3}, 10^{-2}, and 10^{-1} s^{-1}. The gauge size of the static specimens is $15 \times 3.5 \times 2$ mm.

Dynamic tensile tests were carried out on a self-designed Split-Hopkinson tensile bar (SHTB) apparatus whose setup and measuring principle, accounted for in details elsewhere [8–10], are shown in Fig. 1. The specimen, whose shape and size are shown in Fig. 2, was glued to the slots in the ends of input and output bars (4 and 6). As the hammer (1) on the high-speed rotating disk (not drawn in Fig. 1) impacted the block (2), the short metal bar (3), which is made of strain rate-insensitive aluminum alloy and was connected with the block, was deformed to breaking and an approximately rectangular input stress impulse was produced and transmitted through the input bar (4) to the specimen (5). One part of the input impulse was reflected to the input bar and the other part was transferred to the output bar (6). The wave signals were recorded on a transient converter through a superdynamic strain meter.

For the input and output bars made of the same material and having the same area of round cross section, according to the supposition of one-dimension wave and homogeneity of stress and strain in the specimen, the measuring formula of strain $\varepsilon(t)$, strain rate $\dot{\varepsilon}(t)$ and stress $\sigma(t)$ of the specimen are as follows:

$$\varepsilon(t) = \frac{C_0}{L_0}\int_0^t [\varepsilon_i(\tau) - \varepsilon_r(\tau) - \varepsilon_t(\tau)]\,d\tau \qquad (1)$$

$$\dot{\varepsilon}(t) = \frac{C_0}{L_0}[\varepsilon_i(t) - \varepsilon_r(t) - \varepsilon_t(t)] \qquad (2)$$

$$\sigma(t) = \frac{EA}{2A_0}[\varepsilon_i(t) + \varepsilon_r(t) + \varepsilon_t(t)] \qquad (3)$$

where E, A, and C_0 are the Young's modulus, cross-section area, and elastic longitudinal wave speed of input and output bars, respectively. L_0 the length, and A_0 is cross-section area of the tested part of the specimen. Input strain wave $\varepsilon_i(t)$ and reflective strain wave $\varepsilon_r(t)$ are measured by strain gauges (7) on the input bar while the transmissive strain wave $\varepsilon_t(t)$ is measured by strain gauges (7) on the output bar.

Fracture surface of specimens tested at static and dynamic strain rates were studied under S520 scanning electron microscope (SEM), operated at an accelerating voltage of 20 kV.

3. Results

The initial near lamellar microstructure of the investigated alloy is shown in Fig. 3. Fig. 4 presents a typical dynamic tensile curve and corresponding strain rate versus strain curve. Upon tension, the strain rate rises promptly, monotonously, and smoothly. It reaches and maintains at a level approximate to the anticipated value

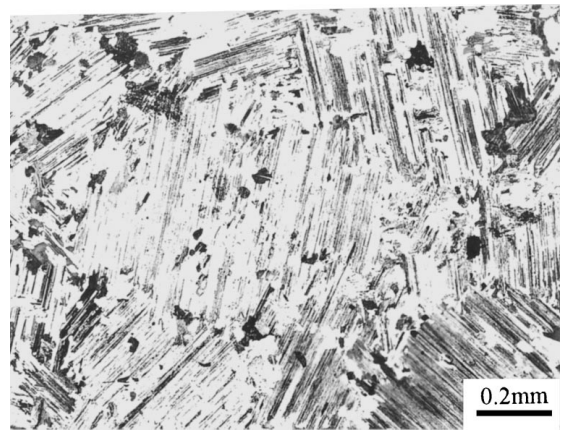

Figure 3 Initial microstructure.

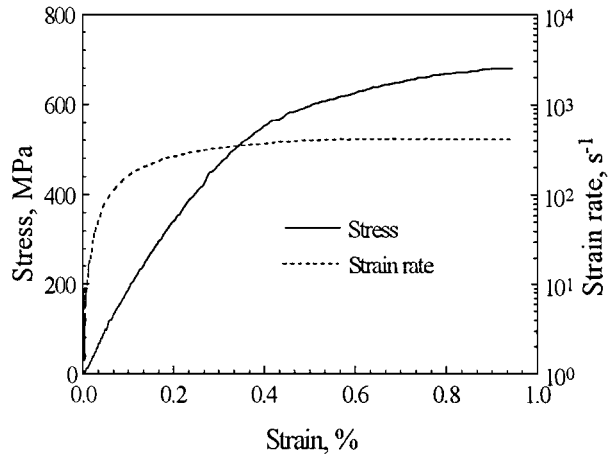

Figure 4 Dynamic tensile curve and corresponding strain rate *vs* strain curve.

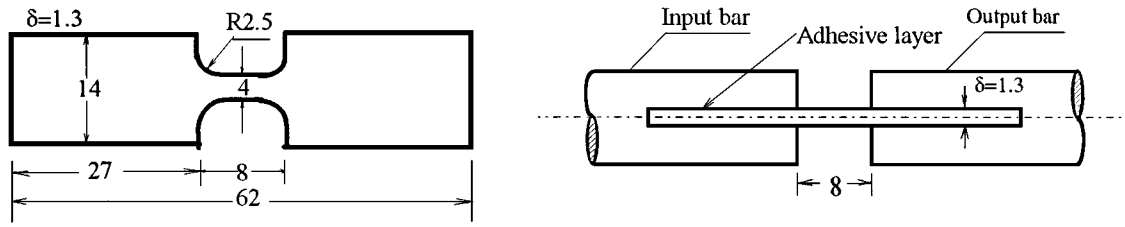

Figure 2 (a) Configuration of specimen and (b) its connection with input and output bars.

TABLE I Strain rate sensitivities of $\sigma_{0.2}$ and σ_b in TiAlMnNb alloy

	$\sigma_s = A + B \ln \dot{\varepsilon}$		$\sigma_d = A + B \ln \dot{\varepsilon}$			$\sigma_d = C + D\dot{\varepsilon}$		
	A, MPa	B, MPa	A, MPa	B, MPa	ρ	C, MPa	D, MPa·s	ρ
$\sigma_{0.2}$	455.0	8.54	429.00	19.33	0.79775	495.52	0.093	0.94931
σ_b	458.5	6.89	460.46	26.96	0.82853	554.06	0.128	0.97341

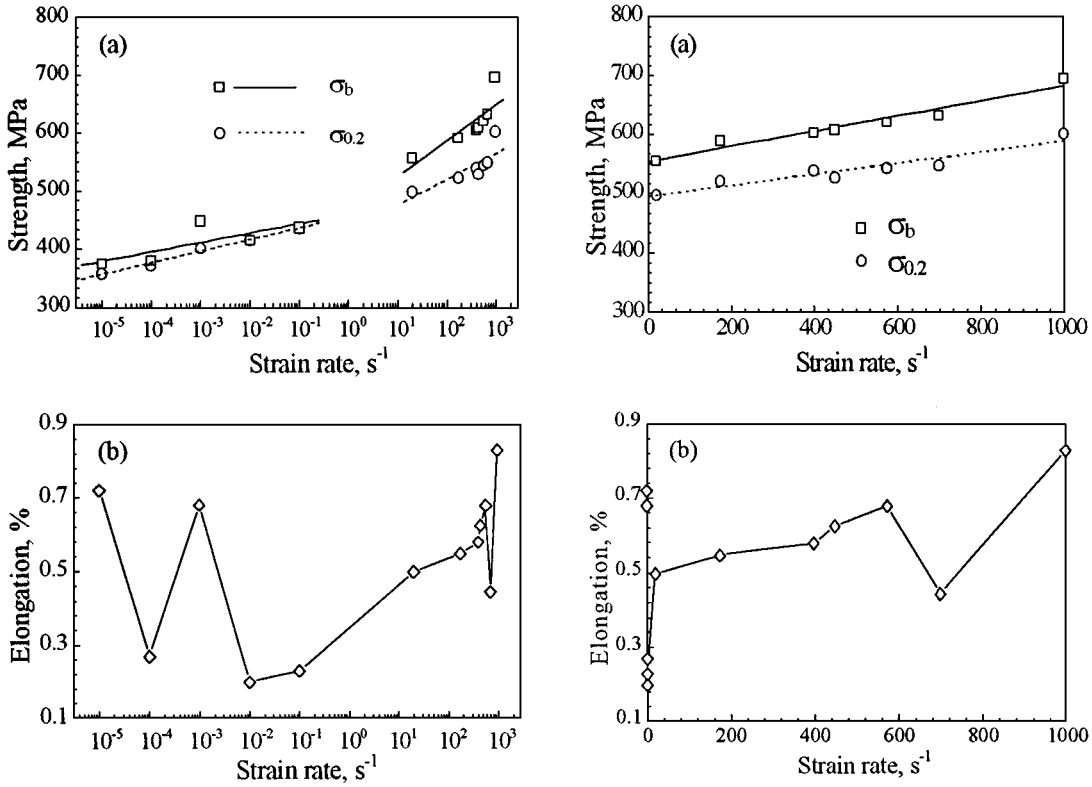

Figure 5 (a) Variation of strengths and (b) elongation with the strain rate in TiAlMnNb alloy.

before the tested specimen yields. Moreover, nonconstitute oscillation, which inevitably shows up in dynamic compressive curves reported in literature [3–6], does not occur in all dynamic tensile curves in this study.

Fig. 5a and Fig. 5b demonstrate the variation of tensile strength (including yield strength $\sigma_{0.2}$ and ultimate tensile strength σ_b) and the elongation δ with the strain rate. Although both $\sigma_{0.2}$ and σ_b increase monotonously with the strain rate in the whole investigated strain rate range, the relationship between static strengths σ_s and the strain rate $\dot{\varepsilon}$ can be better fitted as the following semi-logarithm linear equation

$$\sigma_s = A + B \ln \dot{\varepsilon} \quad (4)$$

where regressive coefficients A and B are listed in Table I, while the relationship between dynamic strengths and the strain rate $\dot{\varepsilon}$ can be better fitted as the following direct linear equation

$$\sigma_d = C + D\dot{\varepsilon} \quad (5)$$

where the regressive coefficients C and D are also listed in Table I. The advantage of Equation 5 over Equation 4 in fitting the relationship between σ_d and $\dot{\varepsilon}$ is reflected by the higher relative coefficients ρ between σ_d and $\dot{\varepsilon}$ than that between σ_d and $\ln \dot{\varepsilon}$ (Table I).

Elongation fluctuates with the strain rate within the investigated strain rate range. It decreases from 0.7% at 10^{-3} s^{-1} to 0.2% between $10^{-2} \sim 10^{-1} s^{-1}$. However, when the strain rate increases further to 20 s^{-1}, the elongation increases again. Dynamic elongation increases slightly with the strain rate except for the abnormally low ductility around the strain rate of 700 s^{-1}. It should be pointed out that owing to the low room temperature ductility of the investigated alloy, the elongation varies within a very narrow range (0.2∼0.8%).

Typical static and dynamic tensile fractographs shown in Fig. 6 exhibit no obvious difference between static and dynamic fracture modes. Both fractographs point to a mixture of predominate transgranular cleavage and minor intergranular failure.

4. Discussion

The less than 1% elongation manifests the brittleness of the investigated alloy. Room temperature static brittleness in TiAl alloy has been attributed to low mobility of dislocation [12], directional bonds of Ti-Ti and Ti-Al [13], low cohesive strength along γ/γ and γ/α_2 interface [14], and environmental embrittlement [15]. The environmental embrittlement in TiAl alloys involves the reaction of Ti and Al atoms with moisture in the air, which generates atomic hydrogen that penetrates into crack tips to reduce overall tensile ductility [15]. It should not be blamed mainly for the low ductility of TiAlMnNb alloy. If the environmental effect played a

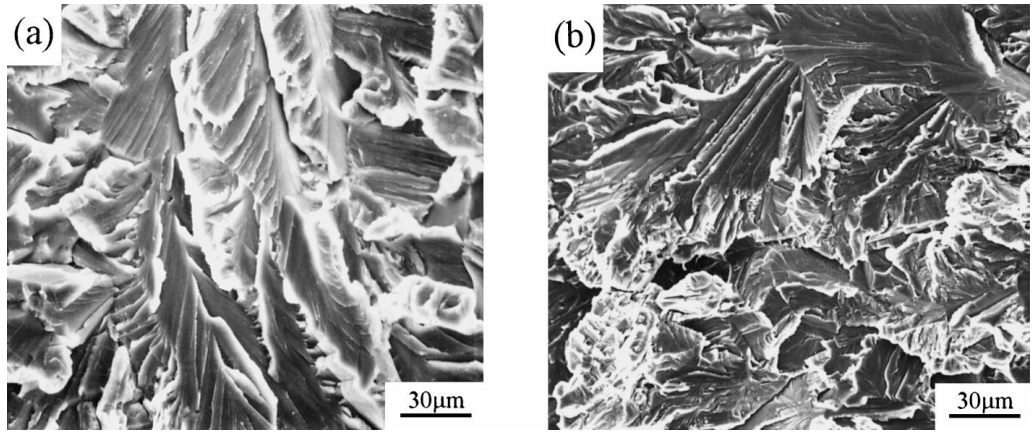

Figure 6 SEM fractographs of TiAlMnNb alloy at the strain rates of (a) 10^{-4} s^{-1} and (b) 10^{3} s^{-1}.

main role, the ductility would increase when the strain rate is raised from 10^{-3} s^{-1} to $10^{-2}\sim10^{-1}s^{-1}$. But, in fact, the elongation decreases from 0.7% at 10^{-3} s^{-1} to 0.2% between $10^{-2}\sim10^{-1}$ s^{-1} (Fig. 4b). The contradiction between the expectation and experimental result rules out the possibility of environmental embrittlement as a main cause for room temperature static brittleness of the investigated alloy.

The dynamic brittleness should not be attributed to the environmental embrittlement, either. As elongation is less than 1% and the strain rate ranges from $20\sim10^{3}$ s^{-1}, the whole dynamic plastic deformation is completed within $10^{-5}\sim10^{-3}$ s. It is hardly possible, in such a short time, for atomic hydrogen to generate through chemical reaction and diffuse into crack tip so as to embrittle the alloy. Although dynamic ductility, on the whole, does increase slightly with the strain rate, it should attributed to another mechanism, which remains to be investigated further.

Fig. 5a indicates that dynamic strength of TiAlMnNb alloy is obviously higher than static strength, which is similar to the compressive cases reported by Chin *et al.* [2] and Maloy *et al.* [3]. The former found that compressive strength jumps from 650∼1050 MPa at 10^{-3} s^{-1} to 1750∼1700 MPa at 500 s^{-1} in Ti–47Al–TiB_2 [2], while the latter found that compressive strength leaps from 900 MPa at 10^{-4} s^{-1} to 1150 MPa at 2000 s^{-1} in Ti–48Al–2Cr [3]. All of these results share a common characteristic of dynamic strengthening, irrespective of tension or compression.

Furthermore, static and dynamic tensile strength of TiAlMnNb alloy varies with the strain rate in different ways: the former observes Equation 4 while the latter observes Equation 5. Equation 4 implies a thermally activated plastic deformation while Equation 5 suggests a viscousdislocation-motion-controlled plastic deformation, which is elucidated as follows:

The strain rate of thermally activated plastic deformation, in analogy to Arrhenius equation, can be written as [16],

$$\dot{\varepsilon} = \dot{\varepsilon}_0 \exp\left\{-\left[\Delta F - \int_0^{\tau^*} V(\tau^*)\,d\tau^*\right]\Big/ kT\right\} \quad (6)$$

where $\dot{\varepsilon}_0$ is a constant, almost independent of the temperature, ΔF is the height of rate-controlling short-range energy barrier to be overcome by a moving dislocation, V is activation volume, and effective stress $\tau^* = \tau - \tau_\mu$, where τ is external applied stress, while τ_μ is long-range internal stress and is almost independent of temperature and the strain rate. To the first approximation, where V does not vary with τ^*, Equation 6 can be converted into

$$\tau = \tau_\mu + \frac{\Delta F}{V} + \frac{kT}{V}(\ln\dot{\varepsilon} - \ln\dot{\varepsilon}_0) \quad (7)$$

Given the temperature, as long as $\tau_\mu + \Delta F/V - (kT/V)\cdot\ln\dot{\varepsilon}_0$, and kT/V are independent of the strain rate, Equation 7 is identical to Equation 4 and also shows a linear relationship between the flow stress and $\ln\dot{\varepsilon}$.

On the other hand, according to dislocation dynamics [16], any moving dislocation dissipates its moving energy to the surrounding, and such dissipation is equivalent to the exertion on it of a drag resistance force, which depends linearly on the strain rate

$$\tau_D = B' \cdot v/b = \eta\dot{\varepsilon} \quad (8)$$

where v is moving velocity of the dislocation, b is the magnitude of its Burgers vector, B′ is called drag coefficient and η macroscopic viscosity. Because the low value (usually between 10^{-5} and 10^{-4} Pa · s) of B′, τ_D is negligible, unless at high moving speed v or high strain rate.

If the strain rate is higher than a critical value $\dot{\varepsilon}_c$ or, equivalently, the externally applied stress is higher than a critical value τ_c, the dislocation overcomes a short-range energy barrier only by external stress, and thermal activation ceases making effect. As a result, the stress component that balances the drag resistance τ_D should be $\tau - \tau_c$,

$$\tau_D = \tau - \tau_c \quad (9)$$

Combination Equation 8 and Equation 9 will result in

$$\tau = \tau_c + \eta\dot{\varepsilon} \quad (10)$$

which is identical to Equation 5 considering $\sigma = f\cdot\tau$, where f is Taylor factor.

The transition from Equation 4 to Equation 5 in the relationship between the flow stress and the strain rate is usually expected to occur around $10^3\,s^{-1}$ or higher [17]. Such expectation is derived from compressive data. Because of the inherent shortcomings in SHPB techniques used to conduct dynamic compressive testing, the tested specimens are not compressed under a constant strain rate, and the yield point is difficult to determine because of the severe nonconstitute oscillation in the early section of dynamic compressive curve. The expectation is, at most, only valid for large plastic strain deformation, where nonconstitute oscillation disappears, and cannot apply to uniform-strain-rate dynamic tensile yield points. In fact, the critical tensile strain rate $\dot{\varepsilon}_c$ in Ti alloy was shown to be around $50\,s^{-1}$ [18], which is approximate to the critical value in this paper. Even for compression, the leap in the compressive strength in Ti–48Al–TiB_2 alloy from 500 MPa at $10^{-3}\,s^{-1}$ to 1000 MPa at $500\,s^{-1}$ by Chin *et al.* [2] can be well interpreted by the transition in rate-controlling mechanism from thermal activation process to viscous motion, which also points to a critical strain rate less than $500\,s^{-1}$, not so high as pointed by [17].

5. Conclusions

1. Dynamic tensile strength σ_d in Ti–47Al–2Mn–2Nb alloy is obvious higher than static strength σ_s at room temperature. There exists a linear relationship between static strength σ_s and the logarithm of the strain rate ($\sigma_s = A + B \ln \dot{\varepsilon}$), and between dynamic strength σ_d and the strain rate itself ($\sigma_d = C + D\dot{\varepsilon}$), which suggests that the rate-controlling dislocation mechanism for plastic deformation changes from thermal activated process under static strain rates to viscous motion under dynamic strain rates.

2. Elongation of the investigated alloy at room temperature fluctuates within a narrow range with the strain rate. Environmental effect is excluded from the main cause for the room temperature brittliness of the investigated alloy.

3. The investigated alloy fractures in a mixed mode of predominant transgranular cleavage and minor intergranular cracking under static and dynamic strain rates.

Acknowledgements

This work was supported by the National Natural Science Foundation of China and United Technologies–Pratt & Whittney Company, USA.

References

1. Y.-W. KIM, *Journal of Metals* **46** (1994) 30.
2. E. S. C. CHIN, T. WEERASOORIYA and P. WOOLSEY, in "*Gamma Titanium Aluminides*," edited by Y.-W. Kim, R. Wagner and M. Yamaguchi (TMS, Warrendale, PA, 1995). p. 451.
3. S. A. MALOY and G. T. GRAY III, *Acta Mater.* **44** (1996) 1741.
4. G. T. GRAY III, *J. de Phys. IV*, **4** (1994) C8-373.
5. S. A. MALOY and G. T. GRAY III, in "Gamma Titanium Aluminides," edited by Y.-W. Kim, R. Wagner, and M. Yamaguchi (TMS, Warrendale, PA, 1995) p. 307.
6. Z. JIM, G. T. GRAY III and Y.-W. KIM, accepted by *Metall. Trans. A*, (1998).
7. L. S. HARBISON, D. A. KOSS and R. J. BOUCIER, in "Titanium '92, Science and Technology," edited by F. H. Froes and I. Caplan (TMS, Warrendale, PA) 1993, p. 1661.
8. Z. WANG, Y. ZHOU and Y. XIA, *J. Mater. Sci.* **32** (1997) 2387.
9. M. CHEN, D. LIN (T. L. LIN), and C. T. LIU, "Influence of Strain rate on Fracture mode of A polycrystalline Ni_3Al," to be published in *Scrip. Mater.*
10. M. CHEN, D. LIN, D. CHEN, D. WANG, Y. XIA and M. YAMAGUCHI, "Dynamic Mechanical Properties of polysynthetically twined (PST) crystals of TiAl with Hard Orientation under Tensile Impact," to be published in *Scrip. Mater.*
11. D. LIN, Y. WANG and C. C. LAW, *Mater. Sci. Eng. A* **239/240** (1997) 369.
12. D. SCHECHTMAN, M. BLACKBURN and H. A. LIPITT, *Metall. Trans.* **5** (1974) 2.
13. M. H. YOO and C. T. LIU, *ISIJ International*, **31** (1991) 1049.
14. Y.-W. KIM, *Acta Metall.* **40** (1992) 1121.
15. C. T. LIU and Y.-W. KIM, *Scrip. Metall. Mater.* **27** (1992) 599.
16. E. NADGORNYI, *Prog. Mater. Sci.* **31** (1988) 1.
17. G. REGAZZONI, U. F. KOCKS and P. S. FOLLANSBEE, *Acta Metall.* **35** (1987) 2865.
18. J. HARDING, *Archives in Mechanics* **27** (1975) 715.

Received 27 July
and accepted 26 August 1998